Hindawi
Journal of Nanomaterials
Volume 2023, Article ID 5484059, 13 pages
https://doi.org/10.1155/2023/5484059

Research Article

Graphene Nanoribbons/Manganese Oxide Nanocomposite Modified Electrode for Detection of Antimicrobial Drug Nitrofurantoin

Ramila D. Nagarajan,[1] Vasanth Magesh,[2] Ashok K. Sundramoorthy,[2] Preethika Murugan,[3] Raji Atchudan,[4] Dhanraj Ganapathy,[2] Sandeep Arya,[5] Abdulnasser Mahmoud Karami,[6] and Mani Govindasamy[7]

[1]*Department of Chemistry, V.V.Vanniaperumal College for Women, Virudhunagar 626001, Tamil Nadu, India*
[2]*Centre for Nano-Biosensors, Department of Prosthodontics, Saveetha Dental College and Hospitals, Saveetha Institute of Medical and Technical Sciences, Poonamallee High Road, Velappanchavadi, Chennai 600077, Tamil Nadu, India*
[3]*Institute of Materials Resource Management (MRM), Augsburg University, Am Technologiezentrum 8, Augsburg 86159, Germany*
[4]*School of Chemical Engineering, Yeungnam University, Gyeongsan 38541, Republic of Korea*
[5]*Department of Physics, University of Jammu, Jammu 180006, Jammu and Kashmir, India*
[6]*Department of Chemistry, College of Science, King Saud University, Riyadh 11451, Saudi Arabia*
[7]*International PhD Program in Innovative Technology of Biomedical Engineering and Medical Devices, Ming Chi University of Technology, New Taipei City 243303, Taiwan*

Correspondence should be addressed to Ashok K. Sundramoorthy; ashok.sundramoorthy@gmail.com and Mani Govindasamy; govindasamy420700@gmail.com

Received 4 November 2022; Revised 3 February 2023; Accepted 14 February 2023; Published 22 April 2023

Academic Editor: Dong Kee Yi

The design and development of a new kind of cost-effective electrode material with excellent selectivity and stability are still a great challenge in the field of electrochemical sensors. Recently, researchers have paid more attention to the electrochemical reduction of nitro compounds due to their hazardous nature. Nitro compounds play a vital role in various industrial applications. However, the direct discharge of nitro compounds to the environment as industrial wastewater is harmful. In this study, a nanocomposite made of 1D graphene nanoribbons decorated with manganese dioxide (GNR-MnO_2) was prepared to fabricate an electrochemical transducer for the determination of nitrofurantoin (NFT) in biofluids. First, 1D GNR was prepared by unzipping of multiwalled carbon nanotubes. Second, the GNR was decorated with MnO_2 by the hydrothermal reduction method. As-prepared GNR-MnO_2 nanocomposite was comprehensively characterized by field emission scanning electron microscopy with EDX, XRD, UV–visible, electrochemical impedance spectroscopy, and cyclic voltammetry. Moreover, GNR-MnO_2-coated glassy carbon electrode (GCE) exhibited good electrocatalytic activity toward NFT. The electroreduction of NFT was found at −0.40 V which was 50 mV lower than bare GCE. GNR-MnO_2 nanocomposite modified GCE showed a well-defined linear reduction peak current for NFT from 10 nM to 1,000 μM. The selectivity of the sensor was also analyzed in the presence of other nitro compounds which confirmed that NFT can be selectively detected at −0.4 V. The GNR-MnO_2 modified electrode was also able to separate reduction peaks of other nitro compounds. In addition, the detection of NFT was carried out in human urine samples with a good recovery of 99.60%–98.60%.

1. Introduction

Synthesis of high-performance catalytic material for the development of compact sensors is on demand. The modern sensor technology has offered many ways to use chemical and biosensors effectively to analyze the environmental, medical, and food samples [1]. The usage of toxic metals, highly poisonous nitro compounds, corrosive acids, and dyes

could cause serious soil and water contaminations. Somehow, these toxic substances have been used in various industrial process, consumer products, and pharmaceuticals (nitro compounds used as drugs). Apart from those, nitroaromatic compounds have been used in the chemical industry, and also in the preparation of explosives, pesticides, dyes, pharmaceutical products, etc. The nitro functional group plays a major role in the chemical and biological activities of nitro-substituted compounds [2]. Due to the strong electronegativity of nitro group, they are harmful to the environment. If the nitro compounds are directly discharged into the water bodies, they can pollute the water and cause carcinogenesis in the human body upon high exposure [3]. Nitrofurantoin (NFT), an antimicrobial drug, is active against the Gram-positive and Gram-negative microbes [4, 5]. Basically, NFT belongs to the family of nitrofuran and it has been used as a medicine for the treatment of coccidiosis and the patients suffering from the deficiency of glucose-6-phosphate [6]. Despite that NFT has excellent antimicrobial activity, still it lacks of metabolic toxicity. The toxicity effect arises from the reduction of nitro group into hydroxylamine and nitroso derivatives by the anionic radical mechanism which helps for the reduction of nitro group. After consumption of NFT as an antimicrobial drug, it gets metabolized in the human body. As a result, 25%–30% of NFT is excreted as in the original form and about 1%–2% excretes through urine as aminofurantoin [7, 8]. Moreover, the reduction process of NFT (nitro group) has the versatile ability to produce the reactive oxygen species. So, the direct discharge of NFT into the ecosystem could be harmful to the environment [9] Thus, it is necessary to monitor the level of NFT concentration in the environmental, biological, and pharmaceutical samples to avoid the harmful effect of NFT [10]. Normally, determination of NFT was carried out by spectrophotometry [11], high-performance liquid chromatography [12], and fluorescence method [13]. These methods have some limitations such as the requirement of pretreatment of samples, time-consuming process, skilled technical persons, and high cost [13]. Recently, electrochemical sensors have been used for the accurate quantification of NFT in environmental samples with high sensitivity and selectivity. In the electrochemical sensors, the electrocatalytic materials play a vital role because of their high surface-to-volume ratio and catalytic activity which helped to achieve high selectivity and sensitivity against the particular analyte in the samples [14]. The nanomaterials were classified as 0D (quantum dots) [15, 16], 1D (carbon nanotube, nanorod, and nanowire) [17, 18], 2D (graphene, MXene, MoS_2, etc.) [19–21], and 3D (nanoparticles with different morphology) [22, 23]. These nanomaterials exhibited unique properties and showed higher electrocatalytic activity in the determination of various analytes [24]. Recently, NFT determination was reported using the graphene oxide/Fe_3O_4 nanorods composite-based sensor and used to determine NFT from 0.005 to 100 μM. This sensor was used to quantify NFT in the pig liver sample [25]. The electrochemical determination of NFT was also studied by barium stannate [26], 3D flower nickel oxide boron doped carbon nitride nanocomposite [27], NiFe anchored functionalized multiwalled carbon nanotube (MWCNT) [4], and $MgFe_2O_4$ nanoparticles [28] based sensors.

Moreover, due to their high electrical conductivity, mechanical properties, hydrophilicity, low cost and biocompatibility, 1D and 2D materials, and their nanocomposite have been used to prepare electrochemical sensors, for examples, graphene [29], boron nitride [30], MXene [31], and graphene nanoribbons (GNRs). GNR is a 1D material which has been used in the development of battery, supercapacitor, and sensors [32]. Recently, the GNR/Co_3O_4 nanocomposite-based sensor was prepared for the selective detection of H_2O_2 [33] and also oxidized GNR showed a good charging capacity of 1,400 mA hr/g in lithium-ion storage [34]. GNR-based sensors were also used to determine epinephrine [32] and nitrogen dioxide [35]. It was found that hybrid material made of GNR and manganese oxide (MnO_2) showed high electrocatalytic activity compared to individual materials.

Herein, for the first time, we demonstrated the application of GNR/MnO_2 nanocomposite modified electrode to selectively determine NFT concentration by the electrochemical reduction process. The GNR/MnO_2 nanocomposite was comprehensively characterized by UV–visible spectroscopy (UV–vis), field emission scanning electron microscopy (FE-SEM), energy dispersive X-ray spectroscopy (EDX) and X-ray diffraction (XRD) analysis. Moreover, the GNR/MnO_2 composite modified electrode was prepared and its electrochemical properties were evaluated against NFT by cyclic voltammetry (CV). GNR/MnO_2 was also used for the selective determination of NFT from 10 nM to 1,000 μM. Finally, selective detection of NFT in human urine sample was demonstrated using a GNR/MnO_2 nanocomposite modified electrode. The effect of various interference on the sensor response was also tested in the presence of a few nitro compounds to investigate the selectivity of the sensor.

2. Experimental

Manganese chloride, NFT, sodium acetate, MWCNTs, sodium hydroxide, and ascorbic acid were purchased from Sigma-Aldrich, India. Sulphuric acid, nitrophenol (NP), nitrobenzene (NB), sodium nitrate, and potassium chloride were purchased from Sisco Research Laboratories, India. The phosphate buffer solution (PBS, pH = 7.4) was prepared using NaH_2PO_4 and Na_2HPO_4 for the sensing of NFT. All the solutions were prepared using the milli-Q-water (18.2 MΩ·cm @ 25 $\pm$ 2°C).

Electrochemical studies were carried out using a three-electrode system with an electrochemical workstation (Model: CHI-760E), USA. The prepared GNR-MnO_2 nanocomposite material was confirmed by UV–vis using a 2000c nanodrop spectrophotometer, NanoDrop Technologies, USA. All the experiments were performed at room temperature (25 $\pm$ 0.2°C). The surface morphologies of GNR and GNR-MnO_2 were examined by high resolution scanning electron microscope (HR-SEM, 2100 plus electron microscope) (JEOL, Japan).

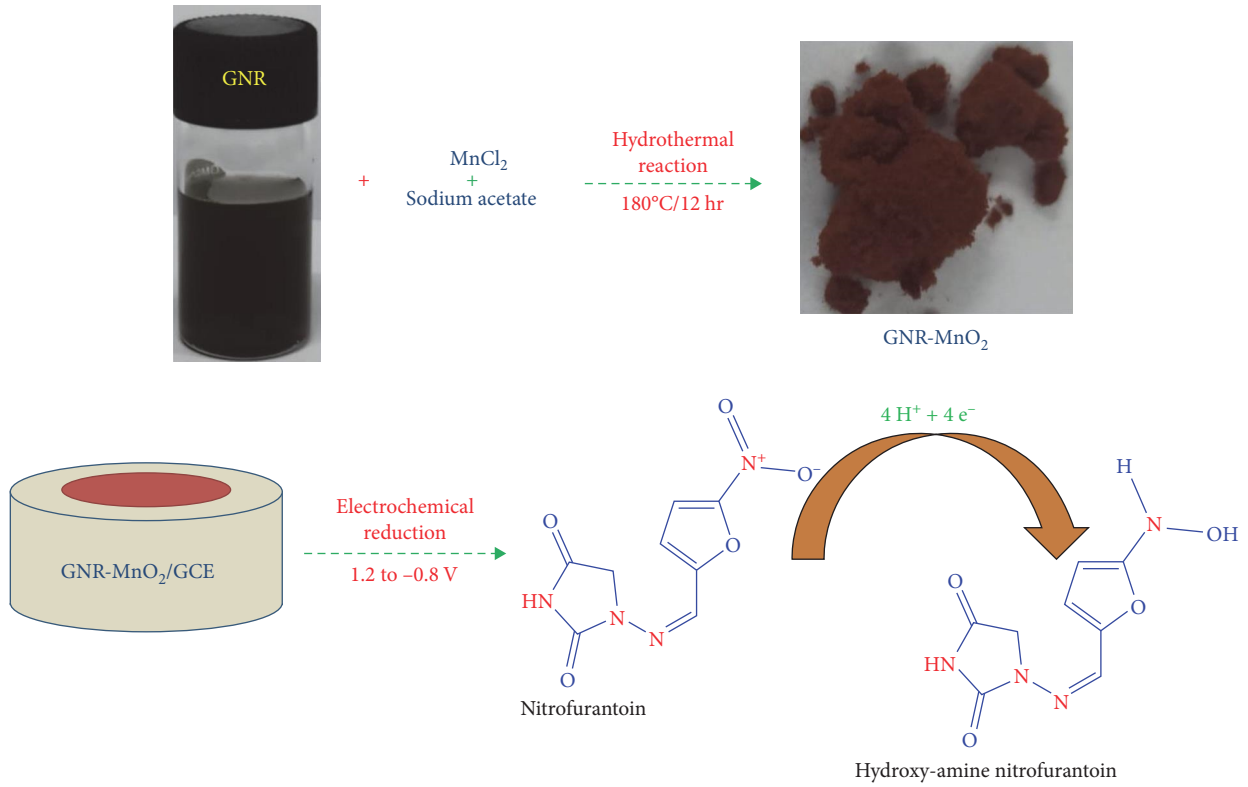

Scheme 1: The graphical representation for the synthesis of GNR/MnO_2 for electrochemical reduction of NFT.

2.1. Preparation of MnO_2. MnO_2 was prepared by hydrothermal method. Briefly, 4 mM $MnCl_2$ was dissolved in ethanol: water (37 + 3 mL) solution and kept for constant stirring at 600 rpm. After that, 5 mM sodium acetate was added with continuous stirring for 1 hr. Further, the reaction mixture was transferred into 100 mL steel-lined autoclave, and the temperature was maintained at 180°C for 12 hr. After the completion of the reaction, brown precipitate was obtained. The brown precipitate was separated by centrifugation method and washed with ethanol and water. Finally, a dark brown MnO_2 powder was obtained and dried at 60°C (Scheme 1).

2.2. Preparation of GNR/MnO_2 Nanocomposite. First, GNRs were prepared as reported elsewhere [33]. From the obtained powder, dispersion of GNRs was prepared with the concentration of 1.5 mg/mL. Second, the prepared GNR dispersion (10 mL) was added into the reaction mixture of $MnCl_2$ (4 mM)/ethanol:water/sodium acetate (5 mM), as given in Section 2.1. The same hydrothermal synthesis procedure of MnO_2 was carried out. The obtained product was washed several times and precipitate was collected after centrifugation and drying at 60°C [36]. Finally, the prepared GNR/MnO_2 nanocomposite was dispersed in 10 mL distilled H_2O (0.5 mg/mL) using a high-frequency ultrasonicator. The same procedure was used to prepare individual MnO_2 and GNR dispersions for control experiments.

2.3. Preparation of GNR/MnO_2 Modified Electrode. The glassy carbon electrode (GCE) was cleaned on the polishing cloth using alumina slurry until a mirror-like surface appeared. Five microliters of GNR or MnO_2 or GNR/MnO_2 dispersion was drop casted on the polished GCE surface and dried at 50°C for 10 min. The GNR/MnO_2 film modified electrode was used for the electroreduction of NFT in PBS. All the electrochemical studies were carried out at room temperature after purging out dissolved oxygen from the buffer solution using nitrogen gas. To study the interference effect, nitro compounds such as nitrophenol, nitroaniline, nitrobenzene, and sodium nitrate were tested on GNR-MnO_2/GCE in the presence of NFT.

2.4. Preparation of Real Sample. The 30 mL of urine sample was collected from the adult (age 25). The collected urine sample was centrifuged at 4,000 rpm for 10 min and the supernatant was collected. Then, the supernatant was diluted at 1 : 1 ratio with distilled H_2O and mixed well for 2 min. It was again centrifuged at 4,000 rpm for 10 min to collect the supernatant and analyzed by amperometry.

3. Results and Discussion

3.1. UV–Vis Analysis of GNR, MnO_2, and GNR/MnO_2 Nanocomposite. Scheme 1 shows the synthesis process of GNR-MnO_2 nanocomposite for the electrochemical reduction of NFT. UV–vis spectrum of as-prepared GNR was recorded which showed a strong absorbance band at 250 nm due to the partially oxidized GNRs (Figure 1(a)) [37]. On the other hand, the prepared MnO_2 showed the two transition peaks at 284 and 380 nm which were related to the d–d metal transition of MnO_2 nanoparticles (Figure 1(b)) [38]. In the case of GNR-MnO_2 nanocomposite, UV–vis spectrum revealed the corresponding MnO_2 absorbance peaks which were red shifted from 284 to 290 and 380 to 400 nm (Figure 1(c)). These

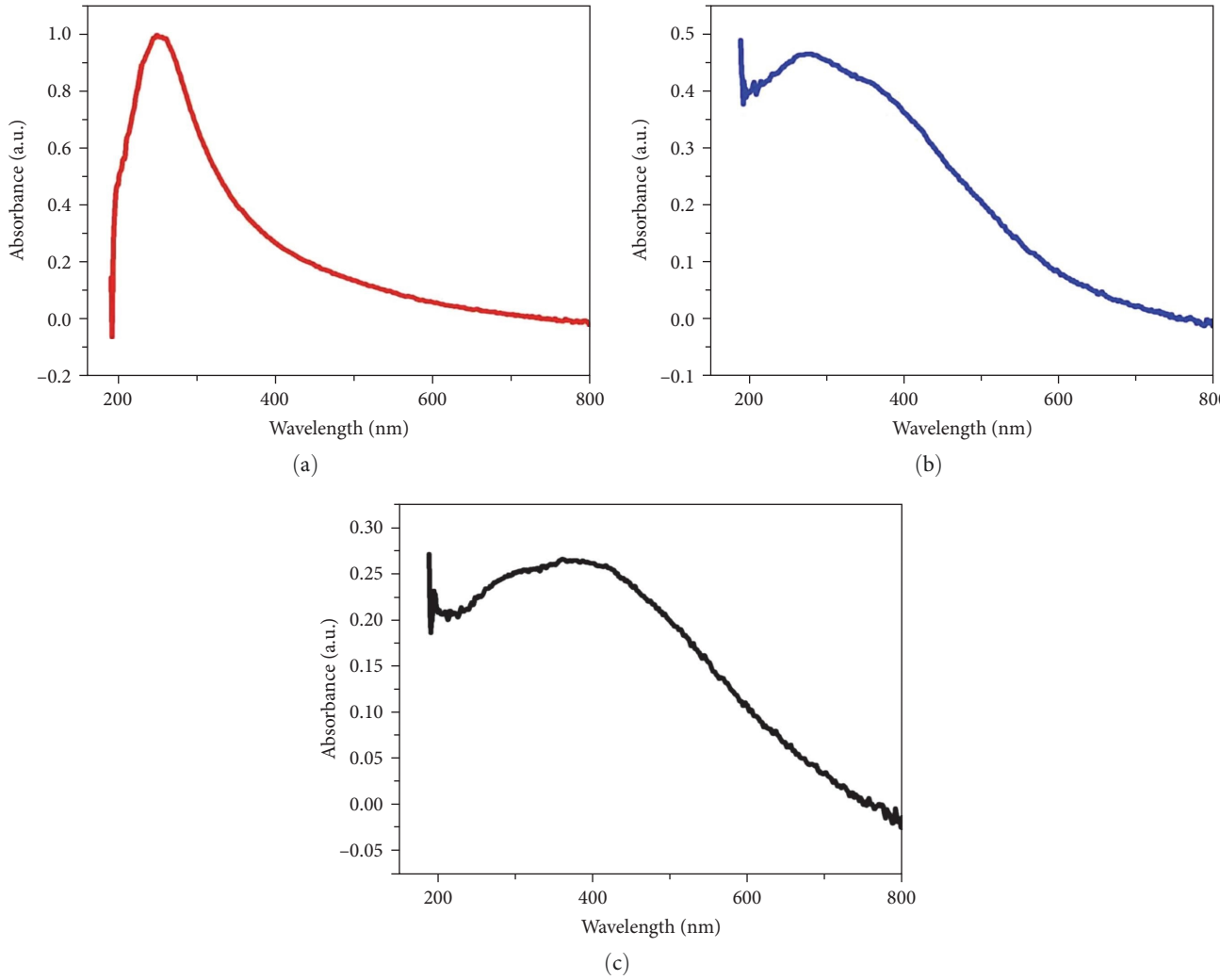

Figure 1: UV–visible spectra of (a) GNR, (b) MnO_2, and (c) GNR-MnO_2 nanocomposite.

observed red shift indicated the interactions between the GNR and the MnO_2 in the nanocomposite [31].

3.2. XRD Pattern Analysis. The GNR, MnO_2, and GNR-MnO_2 nanocomposite samples were analyzed by XRD, as shown in Figure 2. The GNR showed a diffraction peak at 25.4° corresponded to the (002) crystal plane (Figure 2(a)). Another disorder peak was appeared at 42.8°, due to the oxidized GNR [39]. The XRD pattern of MnO_2 showed peaks at (2θ values) 18°, 28.6°, 36.7°, 38.6°, 41.9°, 49.7°, 56.4°, 60.2°, 65.4°, 69.6°, and 72.9° corresponded to (200), (310), (400), (211), (420), (301), (600), (521), (002), (541), and (312) planes, as shown in Figure 2(b). The observed diffraction angles and the planes were corresponded to the α-MnO_2 nanoparticles [40]. Finally, XRD pattern of the GNR-MnO_2 was also recorded which showed the corresponding peaks of GNR-MnO_2. It is worth to note that XRD peaks of the composite sample were slightly shifted toward a higher angle (Figure 2(c)). This observed shift may be due to the presence of synergistic interaction between GNR and MnO_2 in nanocomposite material.

3.3. Surface Morphology Analysis. The surface morphology of as-prepared GNR was characterized and reported by our group [17]. It was shown that MWCNTs were unzipped into GNRs. To study the electrocatalytic activity, MnO_2 nanoparticles were prepared with the average particle sizes of 50–70 nm (Figure 3(a)). To investigate the role of GNRs, the synthesis of MnO_2 was carried out in the presence of GNRs by hydrothermal process. FE-SEM images of as-prepared GNR-MnO_2 nanocomposite confirmed that MnO_2 nanoparticles decorated on the surface of GNR (Figure 3(b)). In addition, the EDX spectra of MnO_2 and GNR-MnO_2 composite were recorded which confirmed the presence of respective elements (Figure 3(c)). In the EDX spectrum of GNR-MnO_2 composite, elements such as Mn (64.15%), carbon (9.67%), and oxygen (26.15%) were present, as shown in Figure 3(d). Thus, both the FE-SEM and EDX analysis were confirmed that MnO_2 nanoparticles successfully incorporated on to GNRs.

3.4. Cyclic Voltammetry (CV) and Electrochemical Impedance Spectroscopy (EIS). The electrode kinetics of the modified electrode was studied by CV and electrochemical impedance

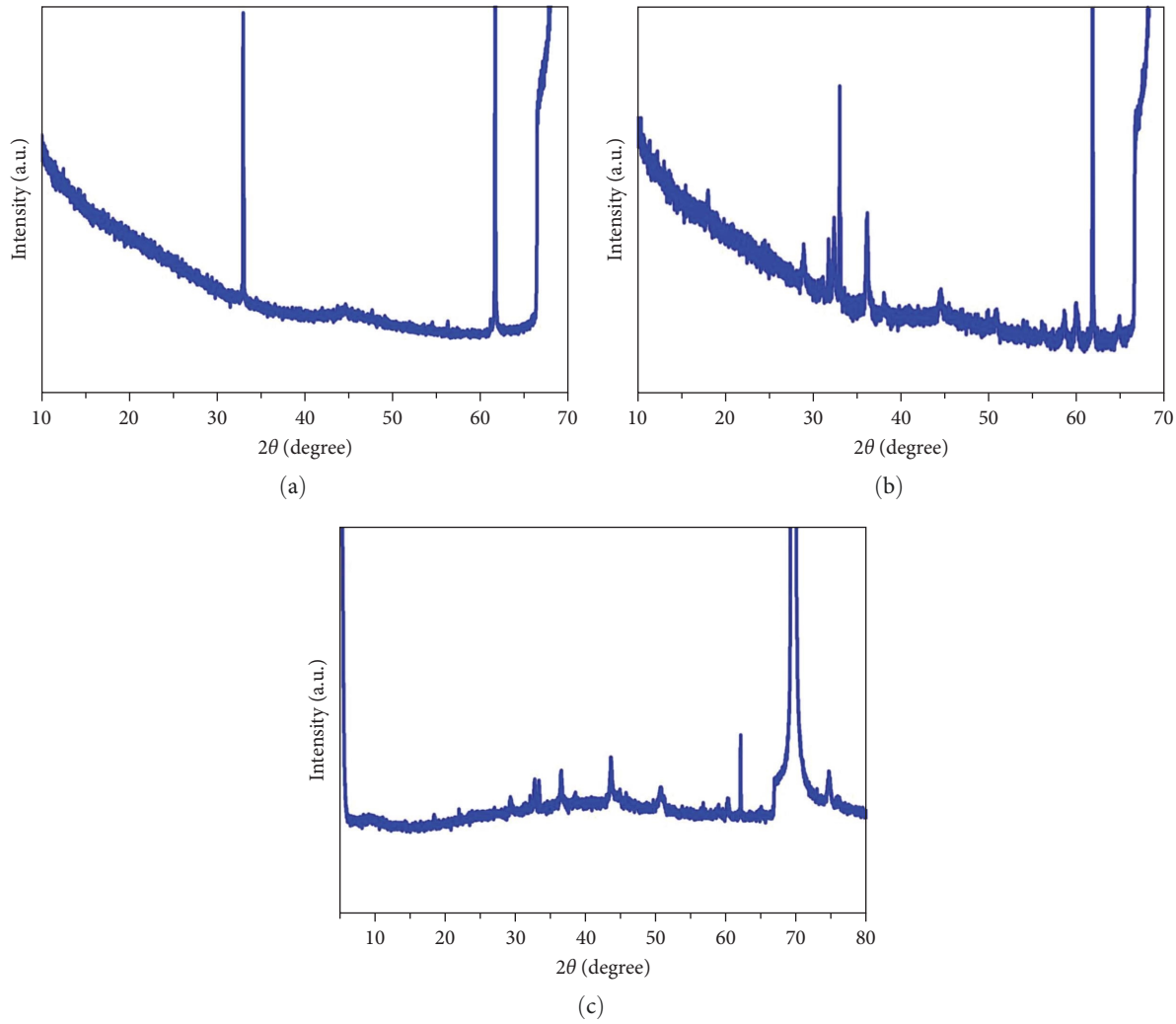

FIGURE 2: XRD spectra of (a) GNR, (b) MnO_2, and (c) GNR-MnO_2 nanocomposite.

spectroscopy (EIS) in 2 mM $[Fe(CN)_6]^{3-}$ with 0.1 M KCl at a scan rate of 50 mV s^{-1}. The bare GCE showed a well-defined redox peak of ferricyanide with the anodic to cathodic peak separation ($\Delta E_p = E_{pc} - E_{pa}$) of 70 mV. However, the GNR-MnO_2 composite modified GCE exhibited a higher peak potential separation value (202 mV) and lower peak current than the bare GCE. It was due to the electrostatic repulsion between the negatively charged GNR-MnO_2 composite and $[Fe(CN)_6]^{3-}$ (Figure 4(a)). Next, both the modified and bare GCEs were analyzed by EIS. The equivalent circuit model was fitted to the EIS spectrum of the GNR-MnO_2/GCE (Figure 4 (b). The obtained solution resistance (R_s) and charge-transfer resistance (R_{ct}) values of bare GCE were 237.9 and 257.1 Ω, respectively. Similarly, the R_s and R_{ct} of GNR/MnO_2/GCE were measured as 225.2 and 4,100 Ω, respectively, in 0.1 M KCl containing 2 mM $[Fe(CN)_6]^{3-}$.The R_{ct} of the GNR-MnO_2/GCE was increased up to 4,100 Ω compared to bare GCE (257 Ω). Hence, it was confirmed that the surface resistance of GCE was increased upon coating of GNR-MnO_2 (Figure 4(b)). The effective surface areas of the electrodes were calculated using CV in $[Fe(CN)_6]^{3-}$. The active surface area for the bare GCE and the modified electrode were 0.07 and 0.126 cm^2, respectively.

3.5. Electrochemical Behavior of Modified Electrodes. For the determination of NFT, different modified electrodes were prepared and tested in 0.1 M PBS. The bare GCE, MnO_2/GCE, GNR/GCE, and GNR-MnO_2/GCE were used to record cyclic voltammograms (CVs) in the potential window between −0.8 V and 1.2 V in PBS. Figure 5(a) (curve i) shows CVs of bare GCE without any peaks. However, after the modification with 5 μL GNR dispersion, GNRs/GCE showed a higher capacitance current than bare GCE (Figure 5(b), curve i). Furthermore, GNR showed a broad redox peak centered at 0.125 V ($E_{pa} \sim 0.2$ and $E_{pc} \sim 0.05$ V). This redox peak was observed due to the presence of quinone functional groups on the surface of GNR which was generated during the unzipping process [41, 42]. Figure 5(c) (black curve i) showed a notable redox peak at 0.8 V ($E_{pc} \sim 0.65$ and $E_{pa} \sim 0.95$ V) with high peak currents which were assigned to MnO_2 [43]. Finally, the GNR/MnO_2/GCE was used to record CVs which exhibited redox peak of MnO_2 with high peak currents due to

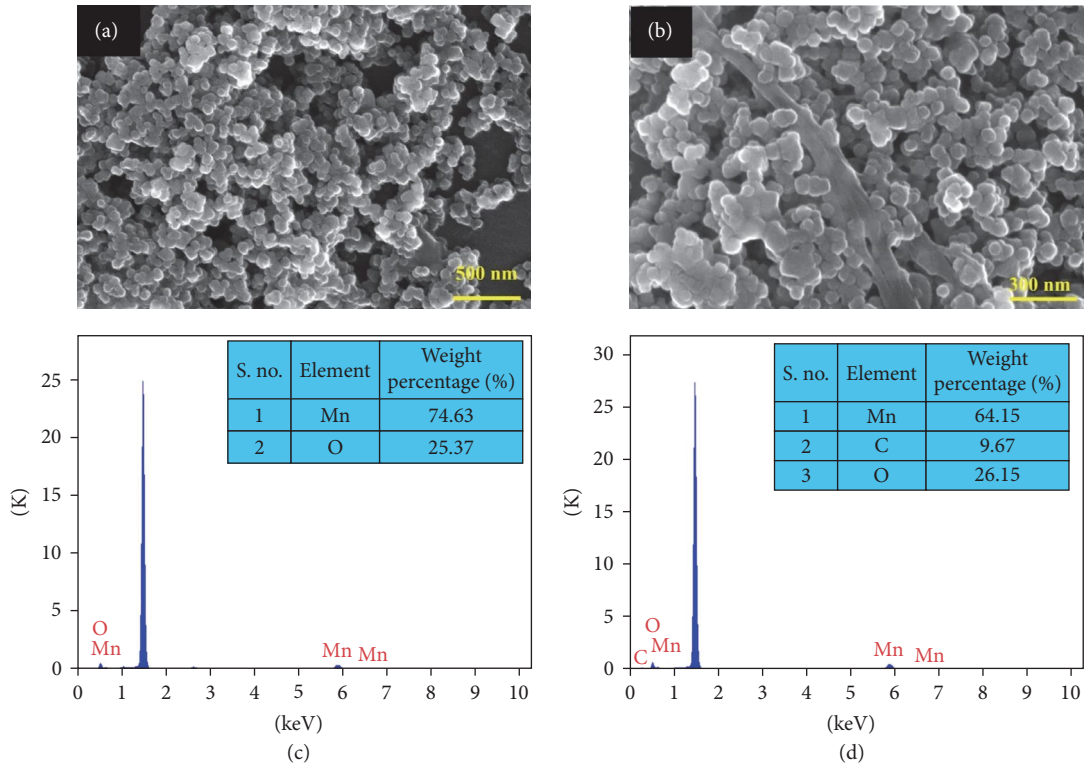

Figure 3: FE-SEM images and the EDX analysis of (a, c) MnO_2 and the (b, d) GNR-MnO_2 nanocomposite.

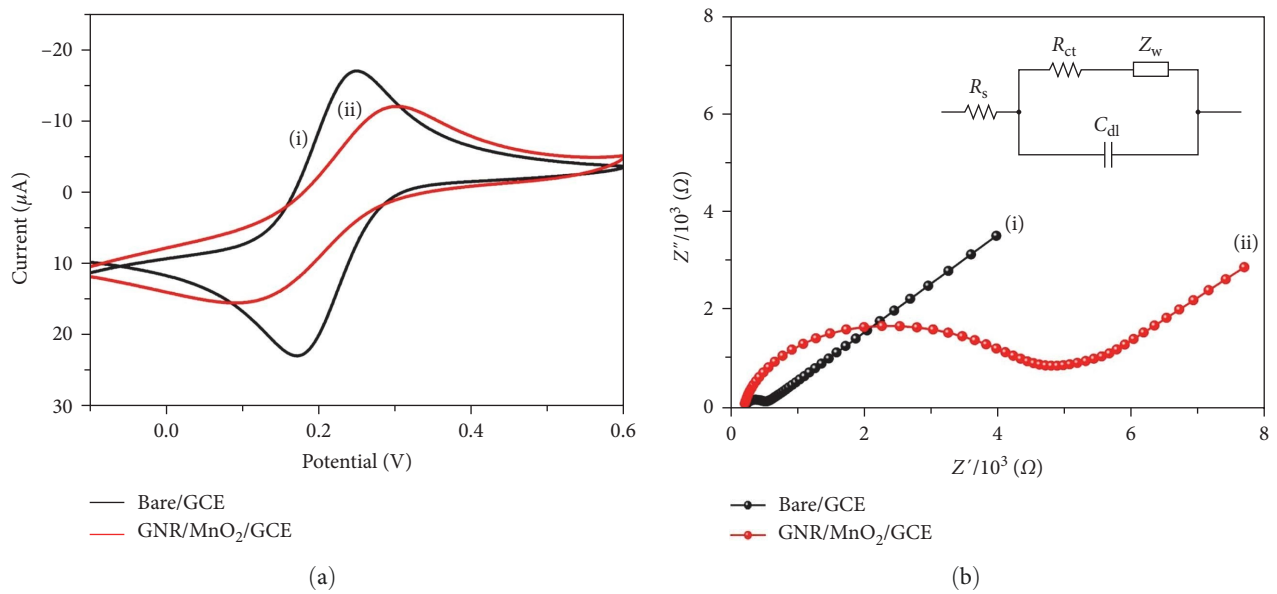

Figure 4: Electrochemical analysis of (a) CV and (b) EIS spectra of (i) bare GCE and (ii) GNR/MnO_2/GCE in 0.1 M KCl with 2 mM $(Fe(CN)_6)^{3-}$ at scan rate of 50 mV s^{-1}. Inset: Randle's equivalent circuit.

the higher active surface area of the composite modified electrode (Figure 5(d)), black curve i). Each one of these modified electrodes were employed in the electroanalysis of NFT.

3.6. Electrochemical Analysis of NFT. Next, CVs were recorded in the presence of NFT on bare GCE which showed the reduction peak at −0.45 V with the peak current of 1.45 μA, (Figure 5(a), red curve ii) [44]. Figure 5(b) (red curve ii) indicated the CVs of NFT reduction peak on GNR/GCE at −0.38 V with the small increment in the peak current of 3.0 μA. Followed by, the MnO_2 modified electrode was used to record CVs with NFT which showed reduction peak at −0.42 V with the cathodic peak current of 2.9 μA (Figure 5(c), red curve ii). Interestingly, the GNR-MnO_2 nanocomposite-coated electrode

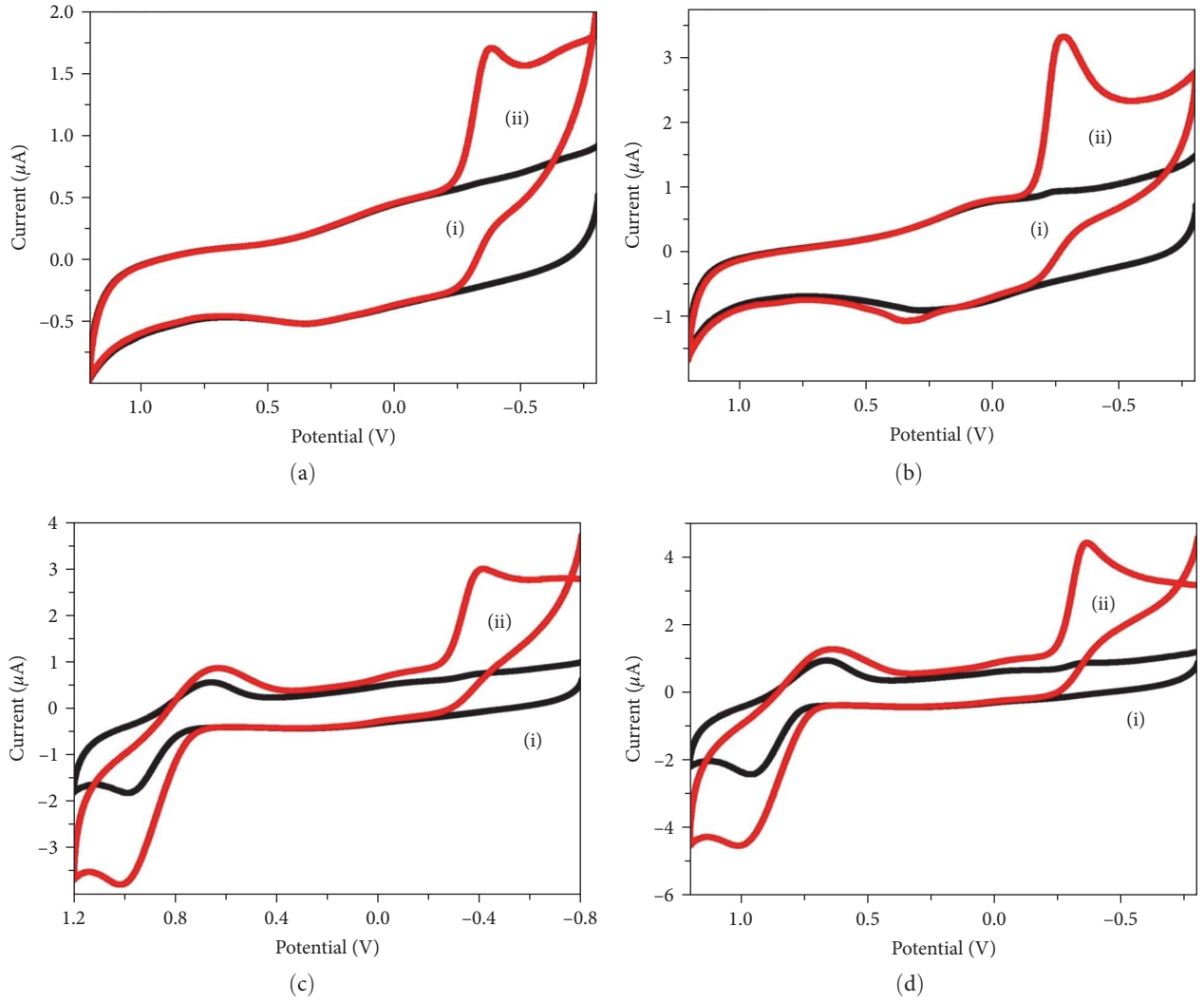

FIGURE 5: CVs were recorded in 0.1 M PBS in the absence (curve i) and presence of 400 μM NFT (curve ii) using (a) bare GCE, (b) GNR/GCE, (c) MnO_2/GCE, and (d) GNR-MnO_2 modified electrode. Scan rate = 50 mV/s.

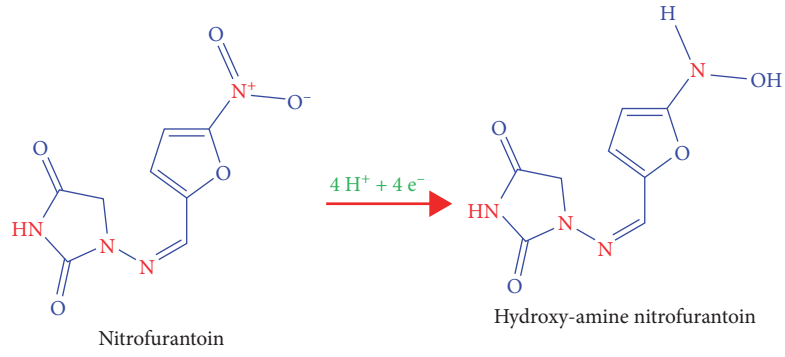

SCHEME 2: The electrochemical reduction mechanism of NFT.

showed the reduction peak of NFT at −0.40 V, with the reduction of overpotential about 50 mV compared to bare GCE with the peak current of 4.5 μA. The higher reduction peak current of NFT observed at the nanocomposite modified electrode indicated the high electrocatalytic activity of the hybrid material. The electrochemical reduction mechanism of NFT is also shown in Scheme 2 [45]. Compared to other reported methods, NFT reduction peak observed at lower potential on GNR-MnO_2/GCE (−0.40 V). For examples, graphene oxide/Fe_3O_4 nanorods composite showed the reduction potential of

Table 1: The comparison of electroanalytical parameters of NFT analysis between the proposed method and other reported methods.

Sr. no.	Electrocatalyst	Linear range (μM)	References
1	NiFe sphere anchored on multiwalled carbon nanotube	0.1–352.4	[4]
2	Graphene/Fe_3O_4 nanorods	0.005–100	[25]
3	$MgFe_2O_4$	0–342.6	[28]
4	Barium stannate	0.01–42.65	[26]
5	GNR/MnO_2 nanocomposite	10 nM–1,000	This work

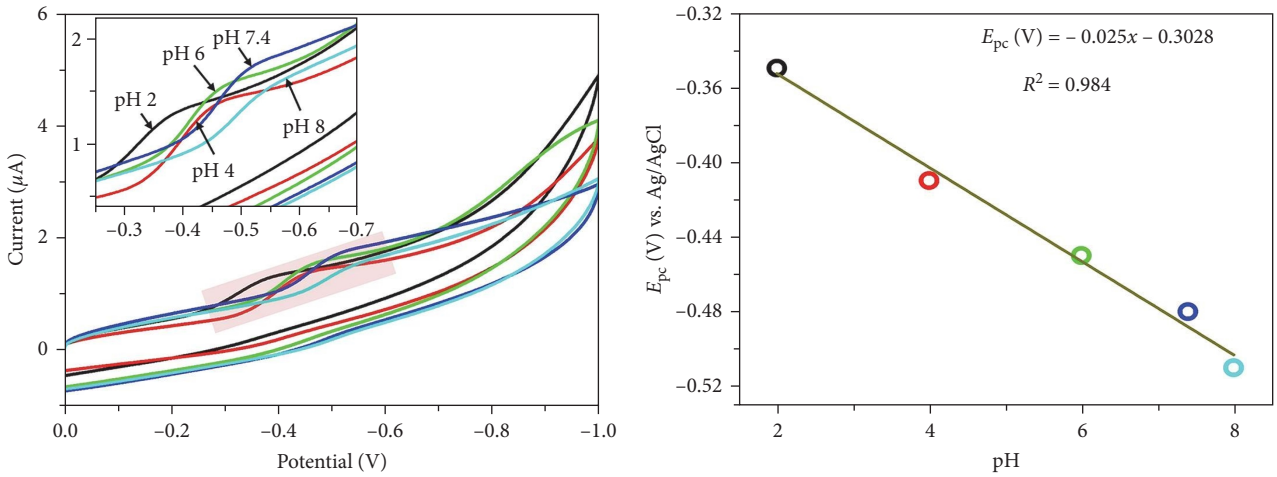

Figure 6: (a) The CVs recorded for the electrochemical reduction of 10 μM NFT at different pH (2, 4, 6, 7.4, and 8). Inset: enlarged highlighted area of (a). (b) The linear plot was established between the pH vs. the NFT reduction potential.

NFT at −0.41 V [25] and the barium stannate modified sensor showed NFT reduction peak at −0.46 V [26] (Table 1). Thus, it is confirmed that the proposed GNR-MnO_2 is a good composite material to develop NFT sensor.

3.7. Effect of pH on NFT Reduction. The pH of the supporting electrolyte on electroreduction of 10 μM NFT was studied by CV in different pH solutions (pH 2, 4, 6, 7.4, and 8). Depending on the pH, the potential of the NFT reduction peak was shifted. When the pH was decreased from pH 8 to pH 2, reduction peak potential was shifted from a higher negative potential to positive potential side, as shown in Figure 6(a). From this pH study, it was found that pH 7.4 exhibited a lower reduction potential with a higher peak current than the other pH solutions. The linear plot between the pH vs. the reduction potential of NFT resulted with a slope value of 25 mV/pH (Figure 6(b)). This value indicated that the electrochemical reduction of NFT undergoes the equal number of protons and electrons. For further studies, PBS with pH 7.4 was chosen as the suitable electrolyte for the analysis of NFT in biological samples [46].

3.8. Effect of Scan Rate. CVs were recorded at different scan rates in 0.1 M PBS containing 200 μM NFT from 20 to 200 mV/s. A linear plot was prepared using the scan rate vs. cathodic peak currents, the peak currents were increased linearly against scan rate without much change in the potential. It indicated that the MnO_2 redox process followed a surface-controlled process. The effect of scan rate was also studied in the presence of 200 μM NFT. The linear graph made between the square root of scan rate and NFT reduction peak current revealed that it was a diffusion-controlled process [5].

3.9. Determination of NFT at GNR/MnO_2 Modified Electrode. Figure 7(a) shows CVs of the GNR/MnO_2 modified electrode in 0.1 M PBS with different concentrations of NFT. The reduction peak currents were linearly increased at the peak potential of −0.40 V with respect to concentration of NFT from 10 nM to 1,000 μM. At the higher concentration, the sensors response attained the steady state. The limit of detection (LOD) for NFT was calculated using Equation (1) as 7 nM [47]:

$$\text{LOD} = 3.3 \times \text{standard deviation of the blank/slope of the calibration curve.} \quad (1)$$

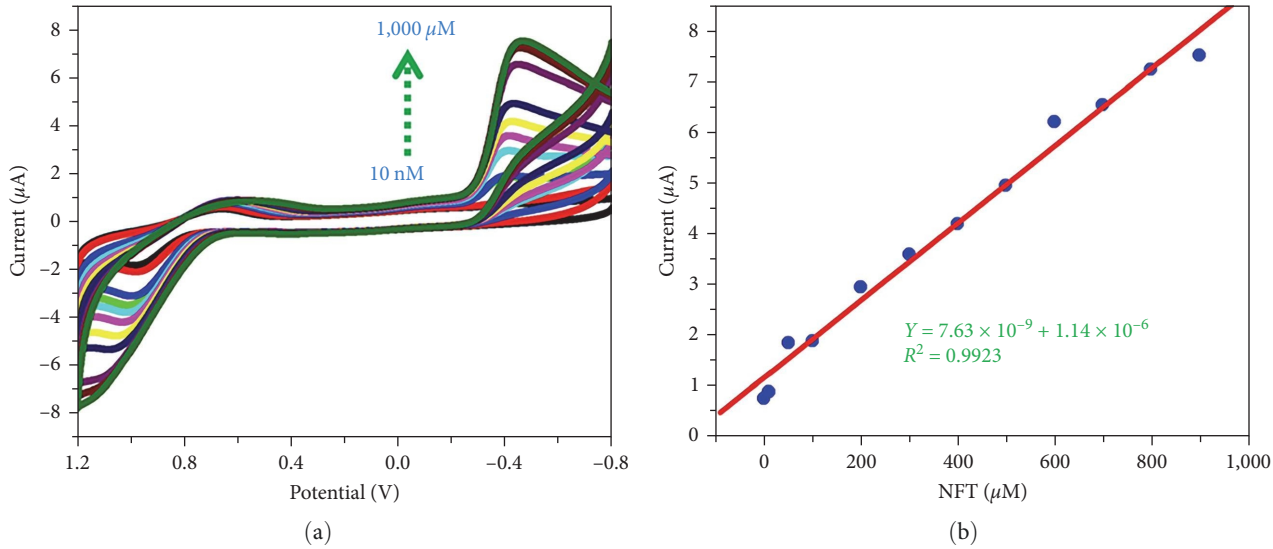

FIGURE 7: (a) CVs were recorded using a GNR-MnO_2 modified electrode with different concentration of NFT from 10 nM to 1,000 μM in 0.1 M PBS at the scan rate of 50 mV/s; (b) calibration graph was made between the concentration of NFT vs. reduction peak currents.

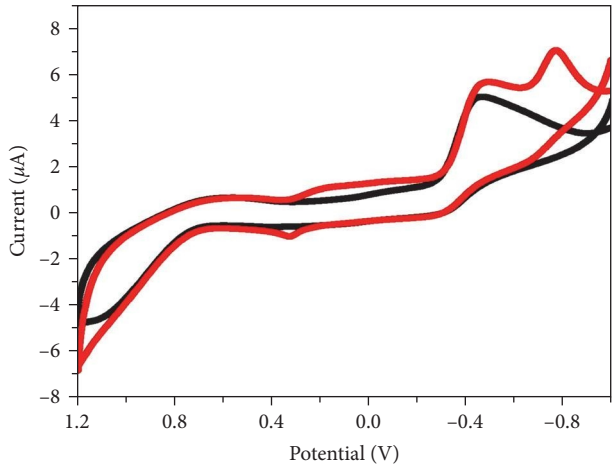

FIGURE 8: CVs were recorded using a GNR–MnO_2/GCE in the presence of 500 μM NFT (black curve) along with 1 μM of other nitro compounds (nitrophenol, nitrobenzene, and sodium nitrate) in 0.1 M PBS at the scan rate of 50 mV/s (red curve).

3.9.1. Interference Analysis. The selectivity of the GNR/MnO_2 sensor toward NFT was also investigated in the presence of other nitro compounds, such as NB, NP, and sodium nitrate. The selectivity of GNR/MnO_2/GCE was tested with 500 μM NFT in the presence of higher concentration of 1 μM NB, NP, and $NaNO_3$ in 0.1 M PBS (Figure 8). From CV analysis, it was found these nitro compounds showed different reduction potential at −0.78, which was well separated from the NFT reduction potential found at −0.40 V. The corresponding reduction peak current of NFT was noted after the addition of each interfering nitro compounds. The sensor response (GNR/MnO_2/GCE) against NFT reduction peak was decreased about 13%. This observation indicated that NFT reduction signal was not affected in the presence of other nitro compounds (Figure 8). Finally, it confirmed that the GNR-MnO_2/GCE had shown good selectivity toward NFT in the presence of other nitro compounds.

3.9.2. Reproducibility, Repeatability, and Stability of the Modified Electrode. Figure 9(a) shows the repeatability data of the GNR/MnO_2 modified electrode which was recorded in 0.1 M PBS with the addition of 10 μM NFT. The same GNR/MnO_2 modified electrode was used to record the reduction peak current of (10 μM) NFT in five different samples with 0.1 M PBS. The observed data indicated that GNR/MnO_2 modified sensor retained the current response of about 99%. Furthermore, to analyze the long-term stability of the sensor, the GNR/MnO_2 modified electrode was used to detect NFT in 0.1 M PBS. After that, the GNR/MnO_2 modified electrode was gently rinsed with distilled H_2O and stored at room temperature for 37 hr. It was later used to measure the NFT in 0.1 M PBS, which indicated that sensors' response was stable up to 92% compared to its initial response for the reduction peak of NFT (Figure 9(b)). Next, the sensor fabrication procedure was repeated to prepare three individual sensors independently (using the same GCE to modify with GNR/MnO_2). As-prepared each sensor was used to determine NFT concentration, which showed the relative standard deviation of 0.49%. This confirmed that our sensor fabrication process was highly reproducible for the fabrication of NFT sensors (Figure 9(c)).

3.9.3. Real-World Sample Analysis. We have also tested our prepared sensor in the determination of NFT in the collected human urine sample. CVs were recorded in 0.1 M PBS with 10 μM NFT before and after spiking with 100 μL of urine sample using GNR-MnO_2 nanocomposite modified electrode (Figure 10(a)). GNR-MnO_2 nanocomposite modified electrode exhibited reduction peak of NFT. However, after spiked with urine, there is a broad peak that was observed between −0.6 and −0.8 V, and no any changes were found at −0.40 V (NFT reduction peak was not increased or decreased). It indicated the absence of NFT in the collected urine sample.

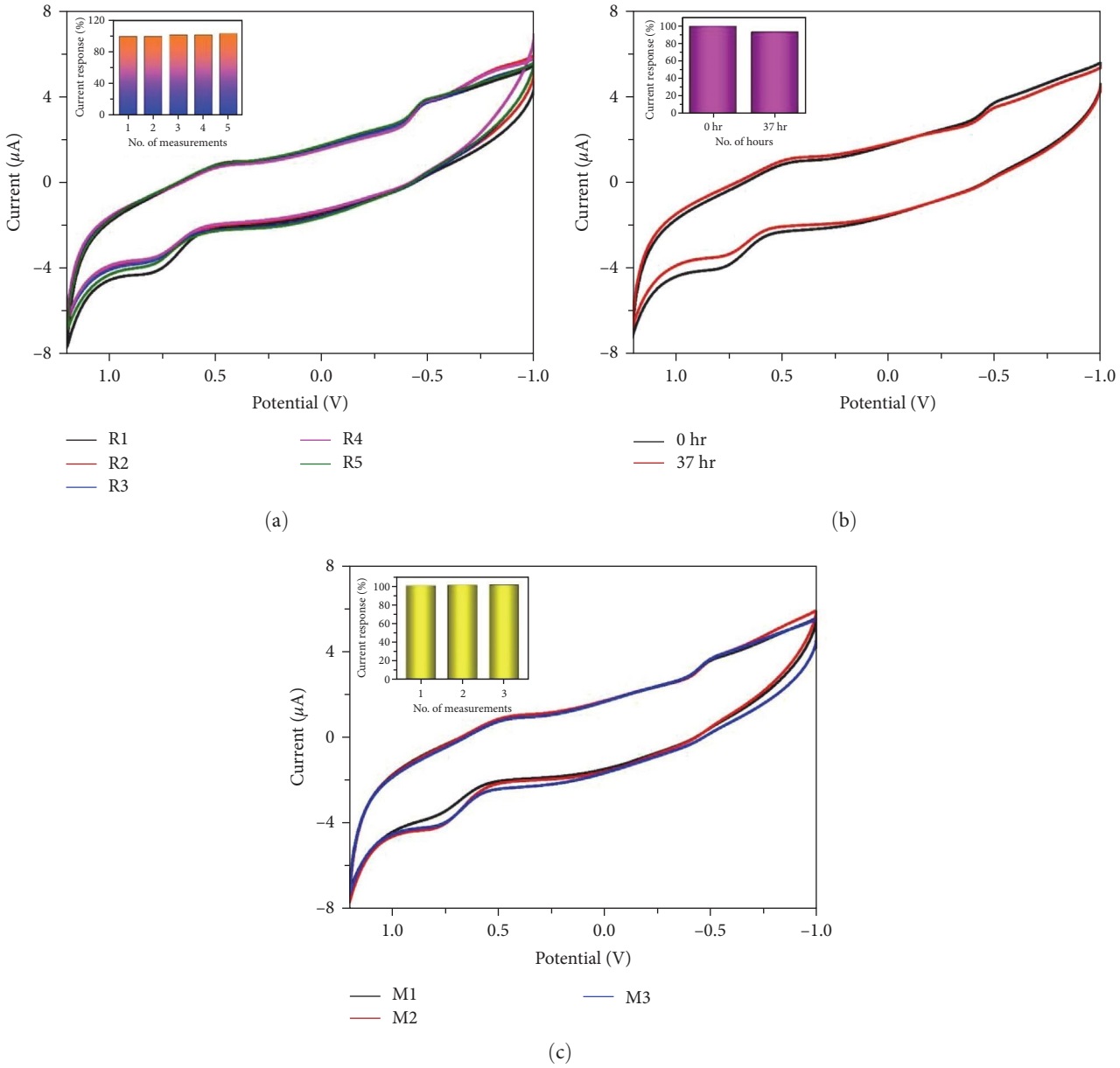

FIGURE 9: (a) The repeatability of the GNR/MnO_2 modified electrode was tested by five repeated measurements in freshly prepared 0.1 M PBS containing 10 μM NFT; (b) the long-term stability of the modified electrode during the analysis of NFT from 0 to 37 hr; (c) CVs of three different GNR/MnO_2 modified electrodes for the NFT reduction. (Inst figures of a–c show the percentage of response of the sensors during the repeatability, stability, and reproducibility measurements).

Moreover, the amperometry (i–t curve) was performed to find out the recovery percentage of NFT in the urine sample after spiked with the standard (Std.) NFT solutions on GNR-MnO_2 nanocomposite modified electrode. Initially, 100 μL of prepared urine sample was added to the 0.1 M PBS, then spiked with standard NFT into the solution mixture (urine + PBS), followed by the addition of three variable concentrations of NFT (2.5, 5, and 10 μM). The amperogram was recorded using the GNR/MnO_2 modified electrode at the applied potential of −0.45 V. No significant current response was observed after the addition of 100 μL of urine. However, after the addition of NFT solutions, sharp reduction currents were observed. Table 2 shows the calculated NFT concentration in the human urine sample using amperometry data after the standard additions of NFT. This shows that the spiked NFT has recovered well in the urine sample (98.6%–99.6%). It was concluded that the GNR/MnO_2 modified electrode can be used for selective detection of NFT in biological samples.

4. Conclusion

We prepared and tested an electrochemical sensor based on GNR/MnO_2 nanocomposite. For this purpose, GNR/MnO_2

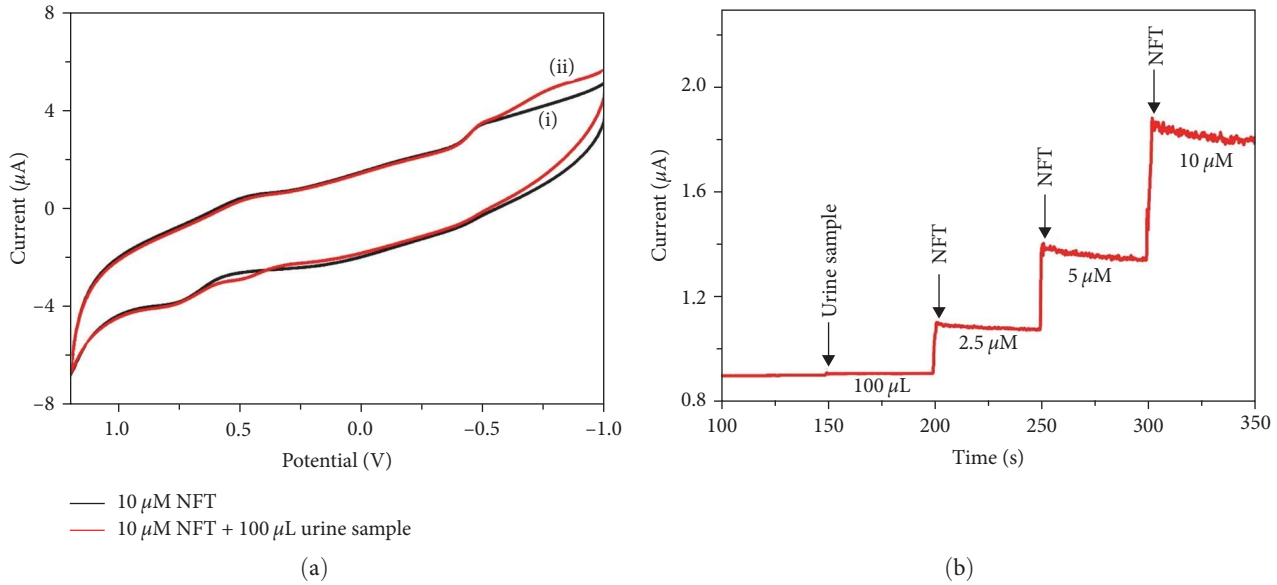

Figure 10: (a) CVs were recorded for the electrochemical reduction of NFT before and after the addition of urine sample using GNR/MnO_2 nanocomposite modified electrode; (b) the amperogram was recorded using a GNR/MnO_2 nanocomposite modified electrode with spiked urine sample and known concentrations of NFT into 0.1 M PBS. The solution was stirred at 750 rpm.

Table 2: Determination of NFT concentration in human urine sample using GNR/MnO_2/GCE sensor.

Sr. no.	Samples	Added (μM)	Found (μM)	Recovery (%)	RSD (%)
1	Human urine	–	–	–	–
2	Std. NFT	2.50	2.49	99.60	0.76
3	Std. NFT	5.00	4.93	98.60	0.66
4	Std. NFT	10.00	9.89	98.90	0.74

nanocomposite was synthesized by hydrothermal method. The synthesized GNR/MnO_2 nanocomposite was comprehensively characterized by UV–vis, EDX, FE-SEM, and XRD. The EDX and XRD data were successfully confirmed the formation of α-MnO_2, GNR, and the GNR-MnO_2 nanocomposite. Moreover, the prepared composite and the individual materials have been applied to prepare electrochemical sensors which were tested in the electroreduction of NFT. The GNR/MnO_2/GCE had reduced the overpotential of NFT reduction reaction and also increased the peak current for NFT, compared to other individual material modified electrodes. The GNR/MnO_2 nanocomposite-based sensor showed a linear response for NFT from 10 nM to 1,000 μM. The selectivity, stability, and repeatability of the GNR/MnO_2/GCE were also investigated which revealed that this sensor can be used for selective detection of NFT in the presence of other nitro compounds with high reliability.

Data Availability

Data will be provided upon request.

Conflicts of Interest

The authors declare that they have no conflicts of interest.

Authors' Contributions

Ramila D. Nagarajan, Vasanth Magesh, and Raji Atchudan contributed equally to this work.

Acknowledgments

The project work was financially supported by the Science and Engineering Research Board (SERB) for funding through CRG/2021/001517. The authors thank the Department of Science and Technology (DST) (International Bilateral Cooperation Division), India, for financial support through "INDO-RUSSIA" project (File No. INT/RUS/RFBR/385). This work was funded by the Researchers Supporting Project Number (RSPD2023R764), King Saud University, Riyadh, Saudi Arabia.

References

[1] R. D. Nagarajan and A. K. Sundramoorthy, "Recent trends in fabrication and applications of wearable bioelectronics for early-stage disease monitoring and diagnosis," in *Macro, Micro, and Nano-Biosensors*, M. Rai, A. Reshetilov, Y. Plekhanova, and A. P. Ingle, Eds., pp. 357–381, Springer, Cham, 2021.

[2] K.-S. Ju and R. E. Parales, "Nitroaromatic compounds, from synthesis to biodegradation," *Microbiology and Molecular Biology Reviews*, vol. 74, no. 2, pp. 250–272, 2010.

[3] U. P. Azad, S. Mahapatra, Divya, A. Srivastava, N. P. Shetti, and P. Chandra, "Electrochemical biosensors for monitoring of bioorganic and inorganic chemical pollutants in biological and environmental matrices," in *Microbial Biodegradation and Bioremediation (Second Edition)*, S. Das and H. R. Dash, Eds., pp. 509–531, Elsevier, 2022.

[4] K.-Y. Hwa and T. S. K. Sharma, "Nano assembly of NiFe spheres anchored on *f*-MWCNT for electrocatalytic reduction and sensing of nitrofurantoin in biological samples," *Scientific Reports*, vol. 10, Article ID 12256, 2020.

[5] K. Sudha, A. Elangovan, S. Senthilkumar, A. Jeevika, and G. Arivazhagan, "Electrocatalytic reduction of nitrofurantoin in biological sample based on assembly of ScMo anchored *f*-MCNNcs modified GCE," *Microchemical Journal*, vol. 172, Part B, Article ID 106943, 2022.

[6] B. Howard and B. Furman, "Nitrofurantoin," in *Reference Module in Biomedical Sciences*, Elsevier, 2018.

[7] J. K. Aronson, Ed. "Nitrofurantoin," in *Meyler's Side Effects of Drugs*, pp. 210–218, Elsevier, Oxford, 16th edition, 2016.

[8] M. M. Radhi, Z. N. Hamad, M. S. Jabir, and S. S. Ezzaldeen, "Electrochemical study of nitrofurantoin at micro- and nanoparticles in blood medium using cyclic voltammetric technique," *Advanced Nano-Bio-Materials and Devices*, vol. 1, no. 2, pp. 78–85, 2017.

[9] B. J. Gardiner, A. J. Stewardson, I. J. Abbott, and A. Y. Peleg, "Nitrofurantoin and fosfomycin for resistant urinary tract infections: old drugs for emerging problems," *Australian Prescriber*, vol. 42, no. 1, pp. 14–19, 2019.

[10] B. Howard, "Nitrofurantoin," in *xPharm: The Comprehensive Pharmacology Reference*, S. J. Enna and D. B. Bylund, Eds., pp. 1–6, Elsevier, New York, 2007.

[11] H. Hadi and M. Mouayed, "Determination of nitrofurantoin in pharmaceutical preparations using flow injection-spectrophotometry," *Journal of the Association of Arab Universities for Basic and Applied Sciences*, vol. 24, no. 1, pp. 74–80, 2017.

[12] D. S. Patel, N. Sharma, M. C. Patel, B. N. Patel, P. S. Shrivastav, and M. Sanyal, "Quantitation of nitrofurantoin in human plasma by liquid chromatography tandem mass spectrometry," *Acta Pharmaceutica*, vol. 63, no. 2, pp. 141–158, 2013.

[13] Y. Wang, T. Chen, Q. Zhuang, and Y. Ni, "Label-free photoluminescence assay for nitrofurantoin detection in lake water samples using adenosine-stabilized copper nanoclusters as nanoprobes," *Talanta*, vol. 179, pp. 409–413, 2018.

[14] L. R. Adil, R. Parui, M. N. Khatun et al., "Nanomaterials for sensors: synthesis and applications," in *Advanced Nanomaterials for Point of Care Diagnosis and Therapy*, S. Dave, J. Das, and S. Ghosh, Eds., pp. 121–168, Elsevier, 2022.

[15] V. Magesh, A. K. Sundramoorthy, and D. Ganapathy, "Recent advances on synthesis and potential applications of carbon quantum dots," *Frontiers in Materials*, vol. 9, 2022.

[16] R. Atchudan, P. Gangadaran, S. Perumal et al., "Green synthesis of multicolor emissive nitrogen-doped carbon dots for bioimaging of human cancer cells," *Journal of Cluster Science*, 2022.

[17] N. Murugan, T. H. V. Kumar, N. R. Devi, and A. K. Sundramoorthy, "A flower-structured MoS_2-decorated f-MWCNTs/ZnO hybrid nanocomposite-modified sensor for the selective electrochemical detection of vitamin C," *New Journal of Chemistry*, vol. 43, no. 38, pp. 15105–15114, 2019.

[18] T. H. V. Kumar, S. K. R. Pillai, M. B. Chan-Park, and A. K. Sundramoorthy, "Highly selective detection of an organophosphorus pesticide, methyl parathion, using Ag–ZnO–SWCNT based field-effect transistors," *Journal of Materials Chemistry C*, vol. 8, no. 26, pp. 8864–8875, 2020.

[19] V. Magesh, A. K. Sundramoorthy, D. Ganapathy et al., "Palladium hydroxide (Pearlman's catalyst) doped MXene ($Ti_3C_2T_x$) composite modified electrode for selective detection of nicotine in human sweat," *Biosensors*, vol. 13, no. 1, Article ID 54, 2023.

[20] S. M. M. Raj, A. K. Sundramoorthy, R. Atchudan, D. Ganapathy, and A. Khosla, "Review—recent trends on the synthesis and different characterization tools for MXenes and their emerging applications," *Journal of the Electrochemical Society*, vol. 169, no. 7, Article ID 077501, 2022.

[21] J. Rajendran, A. K. Sundramoorthy, D. Ganapathy, R. Atchudan, M. A. Habila, and D. Nallaswamy, "2D MXene/graphene nanocomposite preparation and its electrochemical performance towards the identification of nicotine level in human saliva," *Journal of Hazardous Materials*, vol. 440, Article ID 129705, 2022.

[22] A. Ahmed, A. Singh, B. Padha, A. K. Sundramoorthy, A. Tomar, and S. Arya, "UV–vis spectroscopic method for detection and removal of heavy metal ions in water using Ag doped ZnO nanoparticles," *Chemosphere*, vol. 303, Part 3, Article ID 135208, 2022.

[23] K. Gokulkumar, A. K. Sundramoorthy, S.-F. Wang, A. Harikrishnan, and R. A. Alshgari, "High-performance electrochemical sensor based on yttrium sulfide nanoparticles decorated carbon nitride heterostructure for highly sensitive detection of antimicrobial drug in biological samples," *Journal of the Electrochemical Society*, vol. 168, no. 7, Article ID 077516, 2021.

[24] C. Murugan, N. Murugan, A. K. Sundramoorthy, and A. Sundaramurthy, "Gradient triple-layered ZnS/ZnO/Ta_2O_5–SiO_2 core–shell nanoparticles for enzyme-based electrochemical detection of cancer biomarkers," *ACS Applied Nano Materials*, vol. 3, no. 8, pp. 8461–8471, 2020.

[25] B. S. He and J. W. Li, "A sensitive electrochemical sensor based on reduced graphene oxide/Fe_3O_4 nanorod composites for detection of nitrofurantoin and its metabolite," *Analytical Methods*, vol. 11, no. 11, pp. 1427–1435, 2019.

[26] M. Balamurugan, K. Alagumalai, T.-W. Chen, S.-M. Chen, X. Liu, and M. Selvaganapathy, "Simultaneous electrochemical determination of nitrofurantoin and nifedipine with assistance of needle-shaped perovskite structure: barium stannate fabricated glassy carbon electrode," *Microchimica Acta*, vol. 188, Article ID 19, 2021.

[27] T. Kokulnathan and T.-J. Wang, "Synthesis and characterization of 3D flower-like nickel oxide entrapped on boron doped carbon nitride nanocomposite: an efficient catalyst for the electrochemical detection of nitrofurantoin," *Composites Part B: Engineering*, vol. 174, Article ID 106914, 2019.

[28] J. N. Baby, B. Sriram, S.-F. Wang, and M. George, "Effect of various deep eutectic solvents on the sustainable synthesis of $MgFe_2O_4$ nanoparticles for simultaneous electrochemical determination of nitrofurantoin and 4-nitrophenol," *ACS Sustainable Chemistry & Engineering*, vol. 8, no. 3, pp. 1479–1486, 2020.

[29] N. G. Yasri, A. K. Sundramoorthy, W.-J. Chang, and S. Gunasekaran, "Highly selective mercury detection at partially oxidized graphene/poly(3,4-ethylenedioxythiophene):poly(styrenesulfonate) nanocomposite film-modified electrode," *Frontiers in Materials*, vol. 1, Article ID 33, 2014.

[30] R. Jerome and A. K. Sundramoorthy, "Hydrothermal synthesis of boron nitride quantum dots/poly(luminol) nanocomposite for selective detection of ascorbic acid," *Journal of the Electrochemical Society*, vol. 166, no. 9, pp. B3017–B3024, 2019.

[31] R. D. Nagarajan, A. Sundaramurthy, and A. K. Sundramoorthy, "Synthesis and characterization of MXene ($Ti_3C_2T_x$)/iron oxide composite for ultrasensitive electrochemical detection of hydrogen peroxide," *Chemosphere*, vol. 286, Article ID 131478, 2022.

[32] R. Sainz, M. del Pozo, M. Vilas-Varela et al., "Chemically synthesized chevron-like graphene nanoribbons for electrochemical sensors development: determination of epinephrine," *Scientific Reports*, vol. 10, Article ID 14614, 2020.

[33] P. Murugan, A. K. Sundramoorthy, R. D. Nagarajan et al., "Electrochemical detection of H_2O_2 on graphene nanoribbons/cobalt oxide nanorods-modified electrode," *Journal of Nanomaterials*, vol. 2022, Article ID 9866111, 10 pages, 2022.

[34] T. Bhardwaj, A. Antic, B. Pavan, V. Barone, and B. D. Fahlman, "Enhanced electrochemical lithium storage by graphene nanoribbons," *Journal of the American Chemical Society*, vol. 132, no. 36, pp. 12556–12558, 2010.

[35] K. M. Cho, S.-Y. Cho, S. Chong et al., "Edge-functionalized graphene nanoribbon chemical sensor: comparison with carbon nanotube and graphene," *ACS Applied Materials & Interfaces*, vol. 10, no. 49, pp. 42905–42914, 2018.

[36] T. Mounika, S. L. Belagali, and K. T. Vadiraj, "Manganese oxide nanoparticles synthesis route, characterization and optical properties," *Materials Today: Proceedings*, vol. 75, Suppl, pp. 72–76, 2023.

[37] E. Cunha, M. F. Proença, F. Costa et al., "Self-assembled functionalized graphene nanoribbons from carbon nanotubes," *ChemistryOpen*, vol. 4, no. 2, pp. 115–119, 2015.

[38] X. Zhang and W. Yang, "Electrophoretic deposition of a thick film of layered manganese oxide," *Chemistry Letters*, vol. 36, no. 10, pp. 1228-1229, 2007.

[39] J. Li, S. Ye, T. Li, X. Li, X. Yang, and S. Ding, "Preparation of graphene nanoribbons (GNRs) as an electronic component with the multi-walled carbon nanotubes (MWCNTs)," *Procedia Engineering*, vol. 102, pp. 492–498, 2015.

[40] L. Feng, Z. Xuan, H. Zhao et al., "MnO_2 prepared by hydrothermal method and electrochemical performance as anode for lithium-ion battery," *Nanoscale Research Letters*, vol. 9, Article ID 290, 2014.

[41] R. D. Nagarajan, P. Murugan, and A. K. Sundramoorthy, "Selective electrochemical sensing of NADH and NAD^+ using graphene/tungstate nanocomposite modified electrode," *ChemistrySelect*, vol. 5, no. 46, pp. 14643–14651, 2020.

[42] P. Murugan, R. D. Nagarajan, A. K. Sundramoorthy et al., "Electrochemical detection of H_2O_2 using an activated glassy carbon electrode," *ECS Sensors Plus*, vol. 1, no. 3, Article ID 034401, 2022.

[43] S. Thiagarajan, T. H. Tsai, and S. M. Chen, "Electrochemical fabrication of nano manganese oxide modified electrode for the detection of H_2O_2," *International Journal of Electrochemical Science*, vol. 6, pp. 2235–2245, 2011.

[44] N. Nataraj and S.-M. Chen, "An electrochemical assay for the detection of nitrofurantoin based on bismuth titanate enclosed carbon nanofiber in environmental and biological samples," *Journal of Electroanalytical Chemistry*, vol. 887, Article ID 115152, 2021.

[45] S. Velmurugan, S. Palanisamy, T. C.-K. Yang, M. Gochoo, and S.-W. Chen, "Ultrasonic assisted functionalization of MWCNT and synergistic electrocatalytic effect of nano-hydroxyapatite incorporated MWCNT-chitosan scaffolds for sensing of nitrofurantoin," *Ultrasonics Sonochemistry*, vol. 62, Article ID 104863, 2020.

[46] F. Ahmed, T. Kokulnathan, A. Umar et al., "Zinc oxide/phosphorus-doped carbon nitride composite as potential scaffold for electrochemical detection of nitrofurantoin," *Biosensors*, vol. 12, no. 10, Article ID 856, 2022.

[47] E. D. Olsen, "Analytical chemistry, fourth edition (Christian, Gary D.)," *Journal of Chemical Education*, vol. 63, no. 11, Article ID A277, 1986.